Journal of Energy Chemistry 51 (2020) 154–160

Contents lists available at ScienceDirect

Journal of Energy Chemistry

journal homepage: www.elsevier.com/locate/jechem

http://www.journals.elsevier.com/journal-of-energy-chemistry/

Flame-retardant concentrated electrolyte enabling a LiF-rich solid electrolyte interface to improve cycle performance of wide-temperature lithium–sulfur batteries

Zhe Yu[a,b], Jianjun Zhang[b,*], Chao Wang[b], Rongxiang Hu[a], Xiaofan Du[b], Ben Tang[b], Hongtao Qu[b], Han Wu[b], Xin Liu[b], Xinhong Zhou[a,*], Xiaoyan Yang[a,*], Guanglei Cui[b,*]

[a] College of Chemistry and Molecular Engineering, Qingdao University of Science and Technology, Qingdao 266042, Shandong, China
[b] Qingdao Industrial Energy Storage Technology Institute, Qingdao Institute of Bioenergy and Bioprocess Technology, Chinese Academy of Sciences, Qingdao 266101, Shandong, China

ARTICLE INFO

Article history:
Received 7 February 2020
Revised 17 March 2020
Accepted 18 March 2020
Available online 14 April 2020

Keywords:
Flame retardancy
Concentrated electrolyte
LiF-rich solid electrolyte interphase
Lithium–sulfur batteries
Wide temperature

ABSTRACT

Lithium–sulfur batteries have been regarded as the most promising high-energy electrochemical energy storage device owing to the high energy density, low cost and environmental friendliness. However, traditional lithium–sulfur batteries using ether-based electrolytes often suffer from severe safety risks (i.e. combustion). Herein, we demonstrated a novel kind of flame-retardant concentrated electrolyte (6.5 M lithium bis(trifluoromethylsulphonyl)imide/fluoroethylene carbonate) for highly-safe and wide-temperature lithium–sulfur batteries. It was found that such concentrated electrolyte showed superior flame retardancy, high lithium-ion transference number (0.69) and steady lithium plating/stripping behavior (2.5 mAh cm^{-2} over 3000 h). Moreover, lithium–sulfur batteries using this flame-retardant concentrated electrolyte delivered outstanding cycle performance in a wide range of temperatures (−10 °C, 25 °C and 90 °C). This superior battery performance is mainly attributed to the LiF-rich solid electrolyte interphase formed on lithium metal anode, which can effectively suppress the continuous growth of lithium dendrites. Above-mentioned fascinating characteristics would endow this flame-retardant concentrated electrolyte a very promising candidate for highly-safe and wide-temperature lithium–sulfur batteries.

1. Introduction

Lithium–sulfur batteries have attracted a great deal of attention owing to the abundant sulfur resources, environmental friendliness and high theoretical energy density (2600 Wh/kg) [1–3]. However, there are still many intractable problems (such as the combustion of electrolyte, the shuttling effect of polysulfides and the growth of lithium dendrites) needed to be resolved [4–6]. The polysulfides dissolve into the electrolyte and shuttle across the separator to react with the lithium metal anode, leading to a rapid fading capacity and deteriorating long-term cycling stability of lithium–sulfur batteries. Physical/chemical confinement is vital for anchoring polysulfides. The novel separator and cathode material with 3D porous structure is another effective strategy to inhibit the PS shuttling effect [7–13]. Compact and stable LiF-rich solid electrolyte interphase (SEI) is beneficial to suppress the continuous growth of lithium dendrites [14–16]. In addition, LiF is a robust electrical insulator (≈10^{-31} S/cm), which prevent electrons from crossing the SEI layer and allows the conduction of lithium ions [17–19]. Therefore, LiF-rich SEI exhibits superb advantages of enhancing surface diffusion of lithium ions during electrodeposition and inducing a uniform and dendrite-free lithium metal anode. Among all the problems, safety is the top priority considerations [20–22]. As is known to all, the widely used electrolytes of lithium–sulfur batteries are mainly composed of 1,3-dioxolane (DOL) and 1,2-dimethoxymethane (DME). However, relatively low boiling points (75 °C for DOL and 42 °C for DME) may lead to cell failure or hazardous safety events. Hence, advanced electrolyte with superior flame retardancy is vital to develop highly-safe lithium–sulfur batteries [23].

Up to now, a series of advanced electrolytes (such as ionic liquid electrolytes, inorganic solid electrolytes, flame retardant electrolytes) have been fabricated to improve the safety issues of lithium–sulfur batteries. Ionic liquid electrolytes with characteristics of low volatility, thermal stability and flame retardancy are much safer than afore-mentioned conventional ether-

* Corresponding authors.
E-mail addresses: zhang_jj@qibebt.ac.cn (J. Zhang), zhouxinhong@qust.edu.cn (X. Zhou), xyang@qust.edu.cn (X. Yang), cuigl@qibebt.ac.cn (G. Cui).

https://doi.org/10.1016/j.jechem.2020.03.034

based electrolytes. Unfortunately, ionic liquid electrolytes may suffer from high viscosity and high cost [24–27]. Inorganic solid electrolytes have great potential to resolve the shuttling effect of polysulfides. But the manufacturing process is too complex to achieve large-scale production [28–31]. Therefore, flame-retardant electrolytes are better alternative way to improve safety of lithium–sulfur batteries. Generally, flame-retardant electrolytes have two mechanisms proposed to explain the flame retardation: (1) Chemical radical-capturing process, which terminates radical chain reactions responsible for the combustion reaction in the gas phase. (2) Physical process, which build-up an isolating layer between the condensed and gas phases to stop combustion process [32,33]. Trimethyl phosphate and triethy phosphate are representative flame-retardant electrolytes [34–38]. Wang's group reported that lithium–sulfur batteries using triethy-phosphate/lithium bis(oxalato)borate/fluoroethylene carbonate flame-retardant electrolyte exhibited superior cycle performance [39,40]. Apart from trimethyl phosphate and triethy phosphate, other flame-retardant electrolytes were also investigated comprehensively. Yuan Yang's group develop a ε-caprolactam/acetamide based eutectic-solvent electrolyte, which can dissolve all lithium polysulfides and lithiumsulfide (Li_2S_8–Li_2S). In addition, this low-cost eutectic-solvent-based electrolyte is difficult to ignite and thus enhance the safety issues of lithium–sulfur battery. However, the discharge specific capacity of the battery still has a way to go, though [41].

Recently, concentrated electrolytes have received much more attention owing to their unique solvation structure and functionality, such as protection of lithium metal anode, suppression of aluminum current corrosion as well as wide electrochemical window [42–48]. Suo et al. developed a new class of ultrahigh salt concentration electrolyte (7 mol LiTFSI to DOL:DME (1:1 by volume)) to effectively suppress the growth of lithium dendrites and inhibit the shuttling effect of polysulfides of lithium–sulfur batteries [47]. Liu et al. fabricated the high-concentration electrolytes (1:2 LiFSI-TEP) for lithium metal batteries. It was noted that high coulombic efficiency (>99%) and excellent cycling stability can be obtained in Li-Cu half-cells [48]. Recently, Wang et al. reported a series of electrolyte mixtures containing lithium bis(trifluoromethylsulphonyl)imide (LiTFSI) and fluoroethylene carbonate (FEC) based solvents coupled with half cell (NMC/Li) and full cell (C/NMC) for comparing the physical, rheological and conductive properties of electrolyte solvents [49]. But the commercial electrolyte shows better cell performance than 0.75 mol/kg LiTFSI/FEC evidently. As far as we all know, few work on lithium sulfur batteries using concentrated electrolytes was reported. Herein, we proposed a new kind of concentrated electrolyte (6.5 M lithium bis(trifluoromethylsulphonyl)imide (LiTFSI)/fluoroethylene carbonate (FEC)) with superior flame-retardancy and steady lithium plating/stripping behavior. It is also found that such concentrated electrolyte can enable the formation of effective LiF-rich SEI on Li metal anode and then suppress continuous generation of lithium dendrites during long-term operation. As a result, such concentrated electrolyte-based lithium sulfur batteries delivered satisfactory battery performances in a wide range of temperatures (−10 °C, 25 °C and 90 °C).

2. Experimental

2.1. Materials

Propylene carbonate (PC), fluoroethylene carbonate (FEC), Lithium bis(trifluoromethanesulphonyl)imide (LiTFSI) and glass fiber were purchased from Sigma Corporation. LiTFSI was dried in vacuum oven at 140 °C overnight in advance. Other chemical regents were used as received without further purification.

2.2. Sample preparation

1 M LiDFOB/PC and 6.5 M LiTFSI/FEC were stirred at room temperature for 12 h.

PAN (1 g) and sulfur (3 g) were mixed homogeneously and heated at 360 °C in nitrogen (N_2) atmosphere for 6 h, thereby resulting in a PAN@S with a sulfur content of 34.18 wt%, as determined by elemental analysis using a PE 2400 II CHNS/O elemental analysis system (PerkinElmer). The theoretical specific capacity of PAN@S is calculated by theoretical specific capacity of sulfur (1672 mAh g^{-1}) multiplying with sulfur content. The cathode was prepared by blending 80 wt% active material (PAN@S), 10 wt% electronic conductor (super-P) and 10 wt% binder (LA133) with appropriate deionized water and then casting on aluminum foil. After dried under high vacuum at 90 °C for 12 h, cutting the foil into small disks with a diameter of 12 mm. The areal densities of sulfur were 0.7 mg cm^{-2} (−10 °C and 90 °C) and 2.5 mg cm^{-2} (25 °C). All batteries went through activation firstly. Galvanostatically charging/discharging tests were carried out on a Land battery test system (Land CT2001A, Wuhan Land Electronic Co. Ltd, China) in the voltage range between 1.0 V and 3.0 V (vs. Li^+/Li).

2.3. Sample characterization

The performance of Li/Li symmetric cells, Li/Cu cells and S@PAN/Li cells were tested with LAND testing systems. Scanning electron microscopy (SEM, Hitachi S-4800) was employed to characterize the morphology of samples. X-ray photoelectron spectroscopy (XPS) performed on a Thermo Scientific ESCA Lab 250Xi was used to collect the surface components. The ionic conductivity is tested via the electrochemical impedance spectroscopy (EIS) measurement in the frequency range of 100 mHz to 7 MHz. Raman spectra were recorded at room temperature using a Thermo Scientific DXRXI system with excitation from an Ar laser at 532 nm. An in situ optical microscope from the Olympus Corporation was employed to obtain the depositional morphology of lithium metal with different electrolytes in real time so as to better study the interfacial stability. Lithium-ion transference number (t_{Li+}) was calculated using the Bruce–Vincent–Evans equation:

$$t_{Li^+} = [I_{ss} \times (V - I_0R_0)]/[I_0 \times (V - I_{ss}R_{ss})]$$

where V is the applied voltage, I_o and I_{ss} are initial current and steady-state values, respectively, R_o and R_{ss} are initial and steady-state interfacial resistance, respectively.

3. Results and discussion

To further clarify accurate structure of 6.5 M LiTFSI/FEC, we investigated Raman spectra of flame-retardant concentrated electrolyte with different salt concentrations [50,51]. As shown in Fig. 1(a), when increasing LiTFSI concentration to 6.5 M, the peak (the ring breathing mode at 905 cm^{-1}) of FEC gradually diminishes and form Li^+-coordinated FEC (922 cm^{-1}). In the electrolyte with enough FEC, the excess FEC can replace the bound of $TFSI^-$ to form solvent-separated ion pairs (SSIPs). As the increasing mole ratio of LiTFSI, it exists with different forms of solvate complexes from contact ion pairs (CIPs, an FSI^- coordinating with one Li^+) to the aggregates (AGGs, an FSI^- coordinating with two or more Li^+, no free $TFSI^-$), indicating most FEC solvent have been coordinated with Li^+, forming the solvation structure of Li^+-$TFSI^-$-solvent. As a result, there is a little or even scarcely flammable FEC in 6.5 M LiTFSI/FEC electrolyte [52]. The result can also be supported by Fig. 1(b). When increasing LiTFSI concentration, free FEC decreases and forms aggregate (745 cm^{-1}) at 6.5 M LiTFSI/FEC. In which, almost the $TFSI^-$ anions combined with multiple Li^+ cations via strong coulombic interaction.

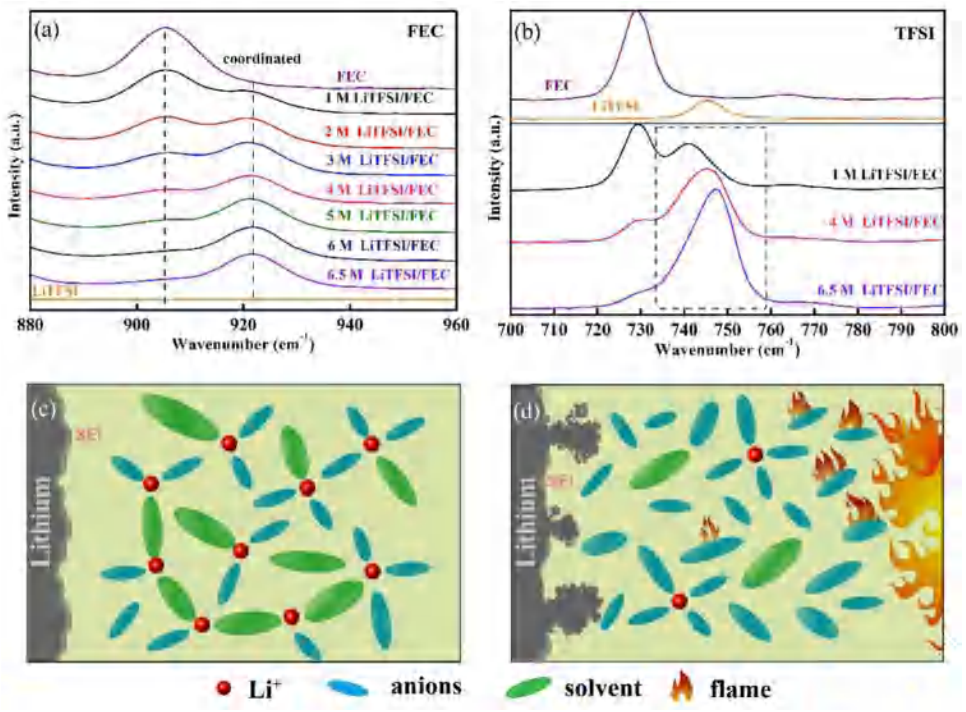

Fig. 1. Raman spectra of LiTFSI/FEC mixtures: (a) 880 cm^{-1} – 960 cm^{-1}, (b) 700 cm^{-1} – 800 cm^{-1}. Illustration of lithium–sulfur batteries using (c) 6.5 M LiTFSI/FEC and (d) 1 M LiDFOB/PC.

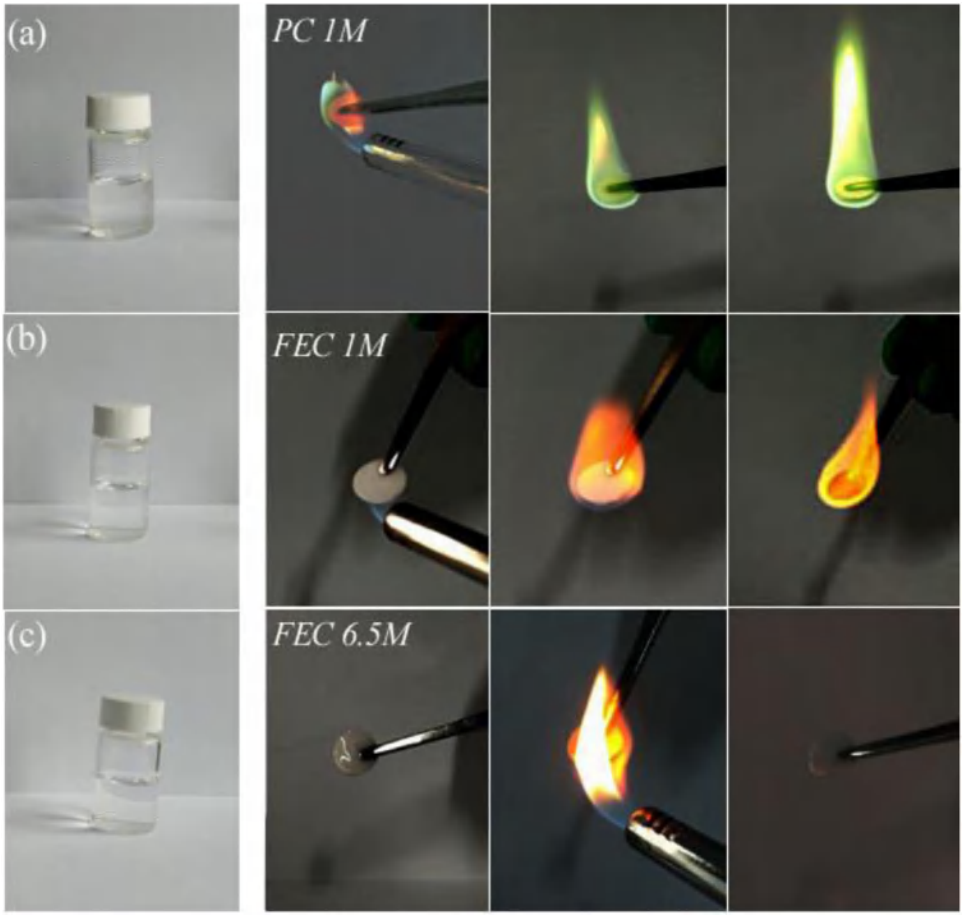

Fig. 2. Flame-retardant photographs of (a) 1 M LiDFOB/PC, (b) 1 M LiTFSI/FEC and (c) 6.5 M LiTFSI/FEC.

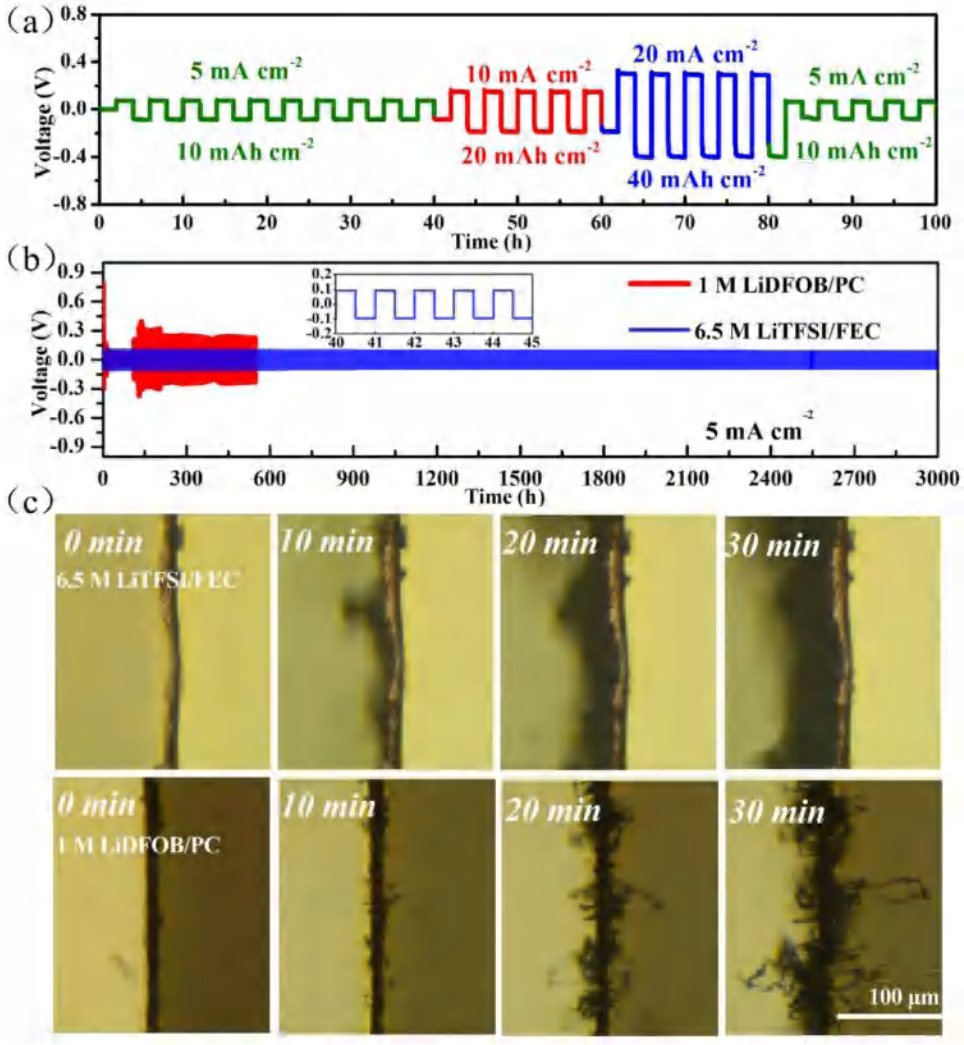

Fig. 3. (a) Voltage profiles of Li/Li symmetrical cell with 6.5 M LiTFSI/FEC electrolyte under different current densities and areal capacities; (b) Voltage profiles of Li/Li symmetrical cells using 6.5 M LiTFSI/FEC electrolyte and 1 M LiDFOB/PC electrolyte cycled at 5 mA cm^{-2} and 2.5 mAh cm^{-2} (the inset is voltage profiles of 6.5 M LiTFSI/FEC electrolyte from 40 h to 45 h); (c) Deposition morphology of lithium-metal to the copper foils using an in situ optical microscope in the Li/Cu half cells with 6.5 M LiTFSI/FEC electrolyte and 1 M LiDFOB/PC electrolyte. (Current density: 2 mA cm^{-2}).

Glass fiber separators soaked 6.5 M LiTFSI/FEC, 1 M LiTFSI/FEC and 1 M LiDFOB/PC were used to evaluate the flame retardancy. As vividly shown in Fig. 2(a and b), once exposured to flame for 1 s, 1 M LiDFOB/PC and 1 M LiTFSI/FEC both ignited immediately and burned, suggesting these two electrolyte are highly flammable. In addition, 1 M LiTFSI/DOL+DME can also be ignited easily and burn continuously (Fig. S1). In a sharp contrast, even exposured to flame for 10 s, 6.5 M LiTFSI/FEC still exhibited excellent flame retardancy (Fig. 2(c)). The origin of flame retardancy of 6.5 M LiTFSI/FEC is as follows: (1) FEC possesses high boiling point (249 °C) and high flash point (120 °C). In addition, there are fluorine in FEC and LiTFSI. Hence, high concentration electrolyte (6.5 M LiTFSI/FEC) was fluorine-contained electrolyte, which was beneficial to enhance the flame retardancy. (2) With respect to 6.5 M LiTFSI/FEC, almost all FEC have been coordinated with LiTFSI to form LiTFSI-FEC pairs, resulting in very scarcely free FEC molecules [42,48,53]. Above-mentioned two factors enable 6.5 M LiTFSI/FEC outstanding flame retardancy.

As demonstrated in Fig. 3(a), it was noted that Li/Li symmetrical cells using 6.5 M LiTFSI/FEC also deliver rate capability at varied current densities and areal capacities (5 mA cm^{-2} and 10 mAh cm^{-2}; 10 mA cm^{-2} and 20 mAh cm^{-2}; 20 mA cm^{-2} and 40 mAh cm^{-2}). As shown in Fig. 3(b), Li/Li symmetrical cells with 6.5 M LiTFSI/FEC exhibited lower polarization voltage and ultra-long cycling stability (over 3000 h) under 5 mA cm^{-2} and 2.5 mA h cm^{-2} as comparing to 1 M LiDFOB/PC and 1 M LiTFSI/DOL+DME (Fig. S10). In addition, a smooth and compact surface on lithium metal anode cycled with 6.5 M LiTFSI/FEC electrolyte was observed after 10 cycles (Figs. S2 and S3). Fig. 3(c) presents the deposition morphology of lithium to the copper foils using an in situ optical microscope in the Li/Cu half cells with different electrolytes. It was found that some visible protuberances appeared on copper foils cycled with 1 M LiDFOB/PC. In a sharp contrast, a compact surface formed on the copper foils in 6.5 M LiTFSI/FEC, suggesting that 6.5 M LiTFSI/FEC is favor to form effective SEI and then suppress the continuous growth of lithium dendrites. Therefore, 6.5 M LiTFSI/FEC could effectively protect metallic lithium anodes against the formation of lithium dendrites. Lithium-ion transference number (t_{Li+}) is an important factor of electrolyte. High t_{Li+} can reduce concentration polarization of lithium batteries. As can be seen from Figs. S4–S6, t_{Li+} (0.69) of 6.5 M LiTFSI/FEC is much higher than that of 1 M LiDFOB/PC (0.38) and 1 M LiTFSI/FEC (0.44). The high t_{Li+} reflects effective transportation of Li ions, which raises the lithium ionic mass trans-

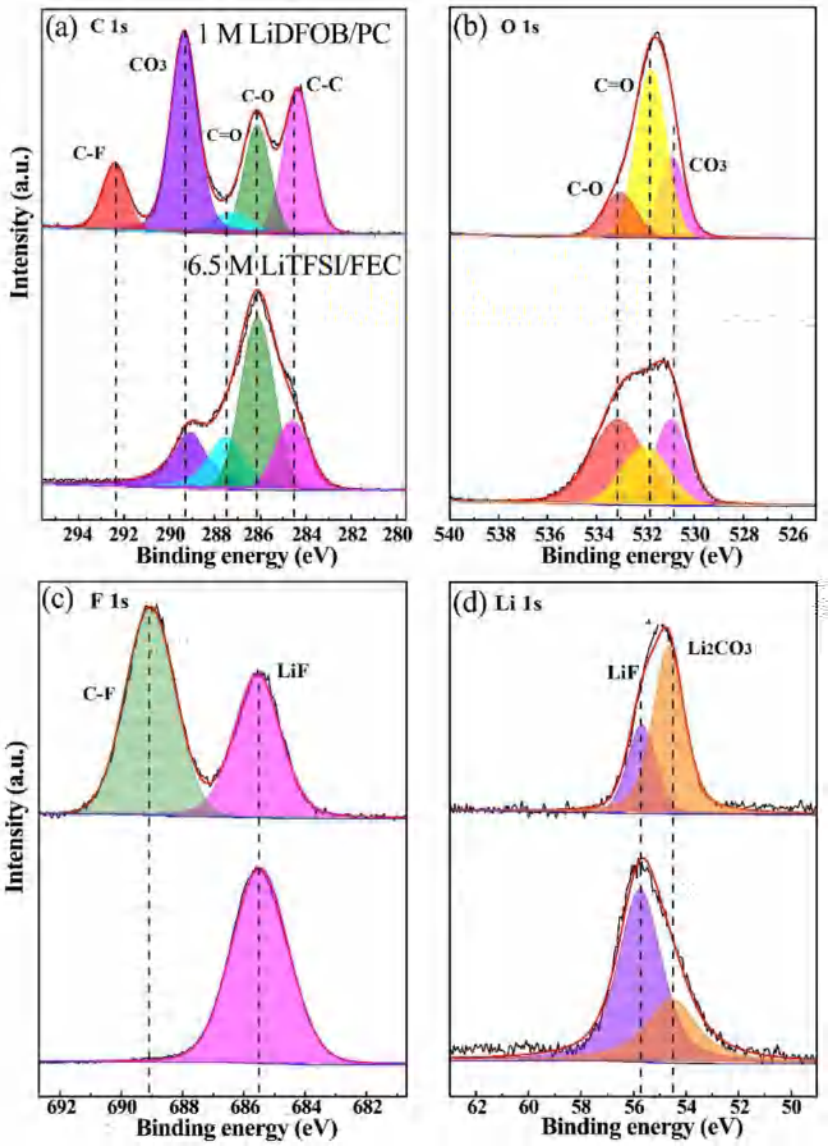

Fig. 4. XPS spectra of cycled Li metal anode disassembled from Li/Li symmetrical cells after 10 cycles with 1 M LiDFOB/PC and 6.5 M LiTFSI/FEC. (a) C 1*s*, (b) O 1*s*, (c) F 1*s*, (d) Li 1*s*.

fer rate between electrolyte and metallic lithium electrode, thereby enhancing the uniformity of lithium deposition and dissolution in charge/discharge process. Hence, high t_{Li+} is expected to protect the Li metal anode effectively [60]. Arrhenius plots of the ionic conductivity of the electrolytes with different salt concentrations in the temperature range of 30 to 90 °C are shown in Figs. S7 and S8. At the room temperature, the electrolytes (LiTFSI/FEC) show ionic conductivity of 0.47, 0.32, 0.28, 0.22, 0.09 and 0.08 mS/cm at different salt concentrations of 1, 2, 3, 4, 5 and 6.5 M, respectively. It can be seen that the ionic conductivity decreases with increasing salt concentration. Linear sweep voltammetry (LSV) is used to measure the oxidation decomposition potential of varied electrolytes. As seen from Fig. S9, electrochemical window of 6.5 M LiTFSI/FEC is 4.9 V, which is higher than that (4.5 V) of 1 M LiDFOB/PC.

As seen from Fig. 4 that the SEI for 6.5 M LiTFSI/FEC mainly consisted of LiF (55.7 eV, Li 1*s*; 685.2 eV, F 1*s*). What's more interesting is that only LiF is found in F 1*s* spectra [54–57]. On the contrary, the content of LiF formed on SEI is fewer for 1 M LiDFOB/PC. There is a chemical equilibrium of "FEC ⇔ VC + HF", FEC may slowly release HF that can react with the alkali SEI components, such as lithium akalycarbonate, lithium alkyoxide, and Li_2CO_3, to form more even and LiF-rich SEI. And a very thin LiF nanolayer can stop electron tunneling but facilitate the Li^+ rapid transport. Zhang's group develop FEC as additives and the lithium metal battery formed a LiF-rich solid electrolyte interphase (SEI), which is compact and stable, and thus beneficial to obtain a uniform morphology of Li deposits [58]. Prof. Wang and his co-workers delivered a high concentration (10 M) of FSI anion enabled interphases of high LiF content on Li-metal anode surfaces [59]. LiF exhibits much higher interfacial energy to Li metal and meanwhile produces a reduction of as much as 0.13 eV in the activation energy barrier for Li diffusion at the electrolyte/Li-metal electrode interface. Thus, the surface diffusivity should be increased by more than two orders of magnitude, which facilitates Li transport along the interface and promotes the formation of a uniform morphology of the deposited Li metal. According to the aforementioned results, the LiF-rich SEI can accommodate suppress the

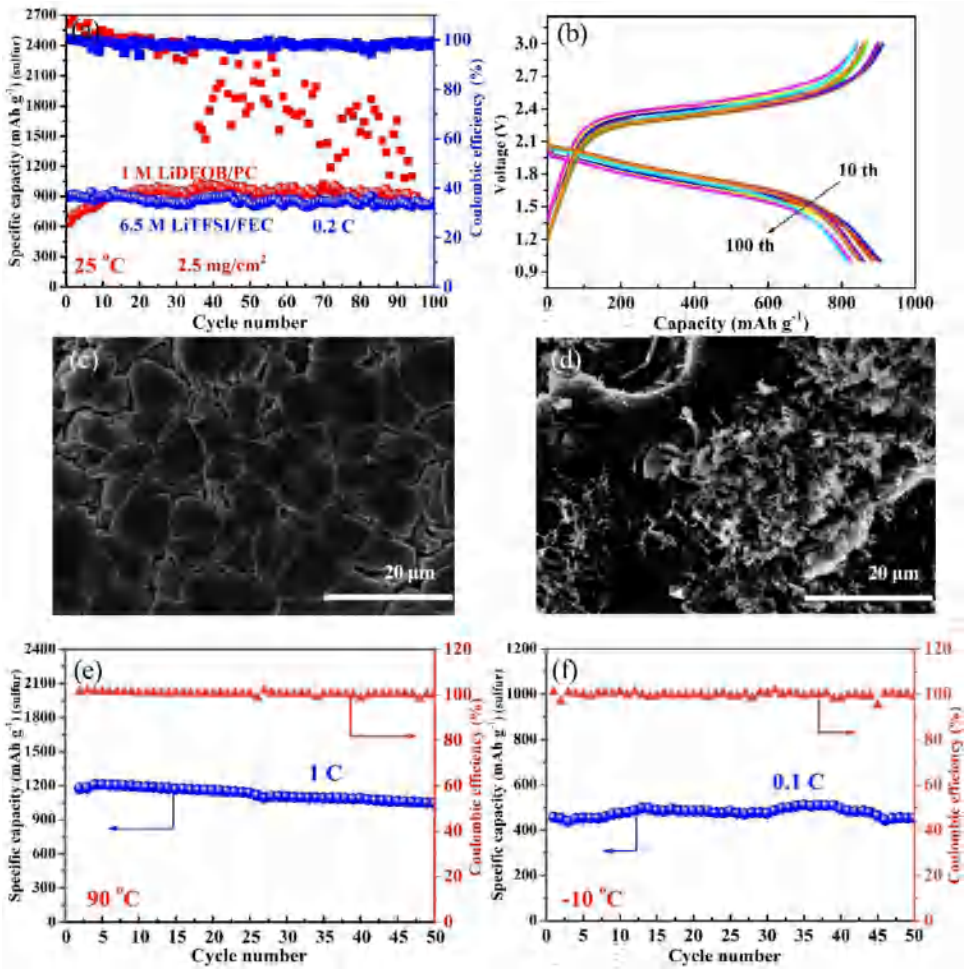

Fig. 5. (a) Cycling stability of lithium–sulfur batteries (2.5 mg/cm^2) using 1 M LiDFOB/PC and 6.5 M LiTFSI/FEC; (b) Typical discharge/charge profiles of lithium–sulfur cells (2.5 mg/cm^2) with 6.5 M LiTFSI/FEC; Typical SEM images of cycled Li metal anode disassembled from lithium sulfur batteries (2.5 mg/cm^2) using (c) 6.5 M LiTFSI/FEC and (d) 1 M LiDFOB/PC; Cycle performance of lithium–sulfur batteries (0.7 mg/cm^2) using 6.5 M LiTFSI/FEC at (e) 90 °C and (f) −10 °C.

growth of lithium dendrites effectively and then enhance electrochemical performance of lithium sulfur batteries when using 6.5 M LiTFSI/FEC.

Fig. 5(a and b) presented the cycle performance and discharge curves of lithium–sulfur batteries with 6.5 M LiTFSI/FEC at 0.2 C. 1 M LiDFOB/PC electrolyte has a higher ionic conductivity and a lower viscosity than 6.5 M LiTFSI/FEC. As a result, the discharge specific capacity of the battery using 6.5 M LiTFSI/FEC may be slightly lower. It is worth noting that the cell with 6.5 M LiTFSI/FEC exhibited high discharge specific capacity (839.1 mAh g^{-1}) and superior cycle performance (capacity retention of 93% after 100 cycles) even at a high sulfur mass loading (2.5 mg/cm^2). Moreover, the coulombic efficiency is higher than that of 1 M LiDFOB/PC (Fig. 5(a)), which is attributed to the steady lithium stripping/plating behavior of 6.5 M LiTFSI/FEC. Striking differences in morphologies of Li deposits in different electrolytes were observed in scanning electron microscopy (SEM) images (Fig. 5c and d). Highly porous/loose structures with extensive dendritic Li growth were observed in 1 M LiDFOB/PC, while, compact aggregates of large nodule-like Li particles without dendrites were observed for 6.5 M LiTFSI/FEC.

In addition, this novel flame-retardant concentrated electrolyte also exhibited satisfactory battery performance at −10 °C and 90 °C. As shown in Fig. 5(e), lithium–sulfur cell exhibited good cycling stability (discharge specific capacity of 981.5 mAh g^{-1} after 50 cycles) at the elevated temperature of 90 °C. The battery with 1 M LiTFSI/DOL+DME delivered a high discharge specific capacity of 600 mAh g^{-1} for five cycles at the low temperature of −10 °C. However, the capacity decays rapidly and the capacity retention is only 33% after 40 cycles. But, in contrast, lithium sulfur battery using 6.5 M LiTFSI/FEC operate well (453.4 mAh g^{-1} after 50 cycles) at the low temperaturte of −10 °C (Fig. 5(f)), which is much better than that of the counterpart (1 M LiTFSI/DOL+DME) (Fig. S11).

Table S1 compares the cycle performance of our results and lithium–sulfur batteries using flame-retardant electrolytes previously reported. As we all know, high temperatures will lead to more serious parasitic side-reactions of lithium–sulfur batteries. Low temperature will lead to the slow reaction kinetics. As shown in Table S1, Lithium–sulfur batteries with flame-retardant 6.5 M LiTFSI/FEC can operate in a wide range of temperatures (−10 °C, 25 °C and 90 °C). The capacity retention is 99.2% after 50 cycles with a capacity attenuation of <0.016% per cycle at −10 °C. In addition, the battery can deliver a discharge capacity above 981.5 mAh g^{-1} at the elevated temperature of 90 °C.

4. Conclusions

In summary, flame-retardant concentrated electrolyte (6.5 M LiTFSI/FEC) was demonstrated to improve safety and battery performances of wide-temperature lithium–sulfur batteries. It was found that such electrolyte exhibited steady lithium plating/stripping behavior (2.5 mAh cm^{-2} over 3000 h). It is worth

noting that the cell with 6.5 M LiTFSI/FEC exhibited high discharge specific capacity (839.1 mAh g^{-1}) and superior cycle performance (capacity retention of 93% after 100 cycles) even at a high sulfur mass loading (2.5 mg/cm^2). In addition, lithium–sulfur batteries with this flame-retardant concentrated electrolyte can also operate well in a wide range of temperatures (−10 °C and 90 °C). At the same time, we also find that this flame-retardant concentrated electrolyte is favor to generate a robust LiF-rich SEI, which can achieve steady lithium plating/stripping and suppress continuous generation of lithium dendrites during long-term cycles. Above-mentioned fascinating characteristics would endow 6.5 M LiTFSI/FEC a promising electrolyte for highly-safe and wide-temperature lithium–sulfur batteries.

Declaration of Competing Interest

The authors declare that they have no known competing financial interests or personal.

Acknowledgments

This original research was financially supported by the National Key R&D Program of China (Grant No. 2017YFE0127600), the National Natural Science Foundation of China (Nos. 51703236 and U1706229), the National Science Fund for Distinguished Young Scholars (No. 51625204), Key Scientific and Technological Innovation Project of Shandong (No. 2017CXZC0505).

Supplementary materials

Supplementary material associated with this article can be found, in the online version, at doi:10.1016/j.jechem.2020.03.034.

References

[1] X. Chen, T. Hou, K.A. Persson, Q. Zhang, Mater. Today 22 (2019) 142–158.
[2] C. Deng, Z. Wang, S. Wang, J. Yu, J. Mater. Chem. A 7 (2019) 12381–12413.
[3] R. Fang, S. Zhao, Z. Sun, W. Wang, H.-M. Cheng, F. Li, Adv. Mater. 29 (2017) 1606823.
[4] Q. Pang, X. Liang, C.Y. Kwok, L.F. Nazar, Nat. Energy 1 (2016) 1–11.
[5] H.-J. Peng, J.-Q. Huang, X.-B. Cheng, Q. Zhang, Adv. Energy Mater. 7 (2017) 1700260.
[6] Z.W. Seh, Y. Sun, Q. Zhang, Y. Cui, Chem. Soc. Rev. 45 (2016) 5605–5634.
[7] W.G. Chong, J.-Q. Huang, Z.-L. Xu, X. Qin, X. Wang, J.-K. Kim, Adv. Funct. Mater. 27 (2017) 1604815.
[8] T.Z. Hou, W.T. Xu, X. Chen, H.J. Peng, J.Q. Huang, Q. Zhang, Angew. Chem. Int. Ed. Engl. 56 (2017) 8178–8182.
[9] L. Li, G. Zhou, L. Yin, N. Koratkar, F. Li, H.-M. Cheng, Carbon N Y 108 (2016) 120–126.
[10] S. Xin, L. Gu, N.-H. Zhao, Y.-X. Yin, L.-J. Zhou, Y.-G. Guo, L.-J. Wan, J. Am. Chem. Soc. 134 (2012) 18510–18513.
[11] X. Chen, W. He, L.-X. Ding, S. Wang, H. Wang, Energy Environ. Sci. 12 (2019) 938–944.
[12] L. Hencz, H. Chen, H.Y. Ling, Y. Wang, C. Lai, H. Zhao, S. Zhang, Nano-Micro Lett. 11 (2019) 1–44.
[13] H. Xiang, J. Chen, Z. Li, H. Wang, J. Power Sources 196 (2011) 8651–8655.
[14] X. Shen, X. Cheng, P. Shi, J. Huang, X. Zhang, C. Yan, T. Li, Q. Zhang, J. Energy Chem. 37 (2019) 29–34.
[15] C. Yan, H. Yuan, H.S. Park, J.-Q. Huang, J. Energy Chem. 47 (2020) 217–220.
[16] Y. Yuan, F. Wu, G. Chen, Y. Bai, C. Wu, J. Energy Chem. 37 (2019) 197–203.
[17] C. Yan, X.B. Cheng, Y.X. Yao, X. Shen, B.Q. Li, W.J. Li, R. Zhang, J.Q. Huang, H. Li, Q. Zhang, Adv. Mater. 30 (2018) e1804461.
[18] C. Yan, H.R. Li, X. Chen, X.Q. Zhang, X.B. Cheng, R. Xu, J.Q. Huang, Q. Zhang, J. Am. Chem. Soc. 141 (2019) 9422–9429.
[19] C. Yan, Y.X. Yao, X. Chen, X.B. Cheng, X.Q. Zhang, J.Q. Huang, Q. Zhang, Angew. Chem. Int. Ed. Engl. 57 (2018) 14055–14059.
[20] C. Hu, J. Yang, H. Wang, Y. Chen, R. Zhang, W. Liu, X. Sun, Environ. Sci. Technol. 7 (2018) 1082–1093.
[21] T. Lei, W. Chen, Y. Hu, W. Lv, X. Lv, Y. Yan, J. Huang, Y. Jiao, J. Chu, C. Yan, C. Wu, Q. Li, W. He, J. Xiong, Adv. Energy Mater. 8 (2018) 1802441.
[22] H. Yang, J. Fu, J. Chen, C. Guo, R. Guo, J. Xie, J. Wang, Environ. Sci. Technol. 7 (2018) 1060–1068.
[23] D.R. Deng, F. Xue, C.-D. Bai, J. Lei, R. Yuan, M. Sen Zheng, Q.F. Dongo, ACS Nano 12 (2018) 11120–11129.
[24] K. Dokko, N. Tachikawa, K. Yamauchi, M. Tsuchiya, A. Yamazaki, E. Takashima, J.-W. Park, K. Ueno, S. Seki, N. Serizawa, M. Watanabe, J. Electrochem. Soc. 160 (2013) A1304–A1310.
[25] A. Vizintin, R. Guterman, J. Schmidt, M. Antonietti, R. Dominko, Chem. Mater. 30 (2018) 5444–5450.
[26] Y. Yan, Y. Yin, Y. Guo, L.-J. Wan, Sci. China Chem. 57 (2014) 1564–1569.
[27] J. Zheng, M. Gu, H. Chen, P. Meduri, M.H. Engelhard, J.-G. Zhang, J. Liu, J. Xiao, J. Mater. Chem. A 1 (2013) 8464–8470.
[28] J. Gao, W. Ren, J. Chen, Environ. Sci. Technol. 6 (2017) 557–571.
[29] D. Lei, K. Shi, H. Ye, Z. Wan, Y. Wang, L. Shen, B. Li, Q.-H. Yang, F. Kang, Y.-B. He, Adv. Funct. Mater. 28 (2018) 1707570.
[30] Y. Liu, P. He, H. Zhou, Adv. Energy Mater. 8 (2018) 1701602.
[31] X. Yu, A. Manthiram, Acc. Chem. Res. 50 (2017) 2653–2660.
[32] J. Zheng, G. Ji, X. Fan, J. Chen, Q. Li, H. Wang, Y. Yang, K.C. Demella, S.R. Raghavan, C. Wang, Adv. Energy Mater. 9 (2019) 1803774.
[33] A. Granzow, Acc. Chem. Res. 11 (1978) 177–183.
[34] H. Ota, A. Kominato, W.J. Chun, E. Yasukawa, S. Kasuya, J. Power Sources 119 (2003) 393–398.
[35] X.M. Wang, E. Yasukawa, S. Kasuya, J. Electrochem. Soc. 148 (2001) A1058–A1065.
[36] X.M. Wang, E. Yasukawa, S. Kasuya, J. Electrochem. Soc. 148 (2001) A1066–A1071.
[37] K. Xu, M.S. Ding, S.S. Zhang, J.L. Allen, T.R. Jow, J. Electrochem. Soc. 149 (2002) A622–A626.
[38] X.L. Yao, S. Xie, C.H. Chen, Q.S. Wang, J.H. Sun, Y.L. Li, S.X. Lu, J. Power Sources 144 (2005) 170–175.
[39] H. Yang, Q. Li, C. Guo, A. Naveed, J. Yang, Y. Nuli, J. Wang, Chem. Commun. 54 (2018) 4132–4135.
[40] H. Yang, C. Guo, J. Chen, A. Naveed, J. Yang, Y. Nuli, J. Wang, Angew. Chem. Int. Ed. Engl. 58 (2019) 791–795.
[41] Q. Cheng, W. Xu, S. Qin, S. Das, T. Jin, A. Li, A.C. Li, B. Qie, P. Yao, H. Zhai, C. Shi, X. Yong, Y. Yang, Angew. Chem. Int. Ed. Engl. 58 (2019) 5557–5561.
[42] V.A. Azov, K.S. Egorova, M.M. Seitkalieva, A.S. Kashina, V.P. Ananikov, Chem. Soc. Rev. 47 (2018) 1250–1284.
[43] O. Borodin, J. Vatamanu, X. Ren, Abstr. Pap. Am. Chem. Soc. 256 (2018) 1155–1184.
[44] L. Suo, Z. Fang, Y.-S. Hu, L. Chen, Chin. Phys. B 25 (2016) 016101.
[45] Y. Yamada, J. Wang, S. Ko, E. Watanabe, A. Yamada, Nat. Energy 4 (2019) 269–280.
[46] Y. Yamada, A. Yamada, J. Electrochem. Soc. 162 (2015) A2406–A2423.
[47] L. Suo, Y.-S. Hu, H. Li, M. Armand, L. Chen, Nat. Commun. 4 (2013) 1–9.
[48] Z. Zeng, V. Murugesan, K.S. Han, X. Jiang, Y. Cao, L. Xiao, X. Ai, H. Yang, J.-G. Zhang, M.L. Sushko, J. Liu, Nat. Energy 3 (2018) 674–681.
[49] Z. Wang, A. Hofmann, T. Hanemann, Electrochim. Acta 298 (2019) 960–972.
[50] J.J. Cael, J.L. Koenig, J Blackwel, Carbohydr. Res. 29 (1973) 123–134.
[51] J. Yu, I.S. Butler, Appl. Spectrosc. Rev. 50 (2015) 152–157.
[52] S.D. Tillmann, P. Isken, A. Lex-Balducci, J. Phys. Chem. C 119 (2015) 14873–14878.
[53] F. Messaggi, I. Ruggeri, D. Genovese, N. Zaccheroni, C. Arbizzani, F. Soavi, Electrochim. Acta 245 (2017) 288–294.
[54] E. Yoo, H. Zhou, ACS Appl. Mater. Interfaces 9 (2017) 21307–21313.
[55] X.L. Fan, X. Ji, F.D. Han, J. Yue, J. Chen, L. Chen, T. Deng, J.J. Jiang, C.S. Wang, Sci. Adv. 4 (2018) eaau9245.
[56] L.L. Wang, J. Ma, C. Wang, X.R. Yu, R. Liu, F. Jiang, X.W. Sun, A.B. Du, X.H. Zhou, G.L. Cui, Adv. Sci. 6 (2019) 1900355.
[57] Z. Peng, N. Zhao, Z. Zhang, H. Wan, H. Lin, M. Liu, C. Shen, H. He, X. Guo, J.-G. Zhang, D. Wang, Nano Energy 39 (2017) 662–672.
[58] X.-Q. Zhang, X.-B. Cheng, X. Chen, C. Yan, Q. Zhang, Adv. Funct. Mater. 27 (2017) 1605989.
[59] X. Fan, L. Chen, X. Ji, T. Deng, S. Hou, J. Chen, J. Zheng, F. Wang, J. Jiang, K. Xu, C. Wang, Chem 4 (2018) 174–185.
[60] C.Z. Zhao, X.Q. Zhang, X.B. Cheng, R. Zhang, R. Xu, P.Y. Chen, H.J. Peng, J.Q. Huang, Q. Zhang, Proc. Natl. Acad. Sci. U S A 114 (2017) 11069–11074.